*J. Fluid Mech.* (2000), *vol.* 423, *pp.* 127–154. Printed in the United Kingdom



# Finite-core hetons: stability and interactions

By M. A. SOKOLOVSKIY[1] AND J. VERRON[2]

[1]Institute of Water Problems of the Russian Academy of Sciences, 3 Gubkina Str., 117735, Moscow, GSP-1, Russia

[2]Laboratoire des Ecoulements Géophysiques et Industriels, UMR 5519 CNRS, BP53 X, 38041 Grenoble Cedex, France

(Received 19 January 1999 and in revised form 8 June 2000)

The dynamics of vertically compensated two-layer vortices (hetons) with finite cores are examined within the context of the quasi-geostrophic approximation on the $f$-plane. The two-layer version of the contour dynamics method is used, and complemented by the so-called contour surgery technique. Special attention is paid to two-heton interactions when the initial locations of the vortex patches are symmetrical. A classification of the different regimes observed is made according to external parameters, namely geometrical parameters and stratification. In this parameter space, novel quasi-stationary states resulting from collisions between two hetons may be observed: (i) formation of a configuration consisting of two-layer vortices moving in opposite directions and, as a special case, a configuration analogous to the 'klapstoss' billiard shot, (ii) absorption of one heton by the other and subsequent movement of a new dipole, (iii) formation of two-layer dipoles, larger than the original hetons, associated with rotating peripheral satellite eddies in their wakes. Some of these results may have implications for the analysis of mesoscale vortices in the ocean.

## 1. Introduction

Mesoscale vortices are now recognized as ubiquitous features of ocean circulation. They most often arise from barotropic and baroclinic instabilities in the strong currents (Gulf Stream, Kuro Shio, Aghulas current, etc.), but they can also appear in the open ocean as a result of local instability, local constraints (e.g. topography), specific forcing features, etc. These coherent structures have a lengthy life and are believed to play a significant role in the redistribution of momentum, heat and salt in the ocean. As a result of their dynamical coherence, the typical distance separating oceanic vortices is often considerable in relation to their own scale (e.g. McWilliams 1984).

The question of the stability of an isolated vortex is of interest *per se* and an unstable structure of this kind can form new coherent vortex structures. Interaction between individual vortices is also of interest as it may result in merging, that is, the appearance of new vortex structures. Interaction between vortices that are initially far apart is possible because of their ability to propel themselves, even in the absence of external influences. For example, Gryanik (1983), Hogg & Stommel (1985*a*, *b*) and Young (1985) have successfully modelled the simplest mechanisms of vortex interaction in the framework of the theory of discrete geostrophic vortices. Moreover, the notion of a *baroclinic vortex pair* (Gryanik 1983) and a *heton* (Hogg & Stommel 1985*a*) – a vortex pair (or dipole) which is formed from discrete eddies located in different layers of a two-layer liquid – appeared to be fruitful when studying trajectories of real vortices in atmosphere and ocean (Gryanik & Tevs 1989, 1997).

The heton concept can be generalized to the case of finite-core two-layer vortices comprising finite size eddies, with constant potential vorticities (PV) of opposite sign in each layer. Such cases are referred to as FAVR (finite area vorticity regions) (e.g. Morel & Carton 1994) or finite-core vortices (Valcke & Verron 1993, 1996, 1997). In this case, in addition to the dimensionless space parameter $l = D/\lambda$, which is characteristic of discrete vortices ($D$ is half the distance between the vortices, and $\lambda$ is the Rossby radius of deformation), a new parameter $\gamma = R/\lambda$ appears, where $R$ is the horizontal scale measuring the size of the vortex patch which is typically its radius. The finite-core vortex, unlike its discrete counterpart, may become unstable with respect to small disturbances and break into smaller vortex structures.

Oceanic observations of coherent eddies and eddy breaking have been conducted, for example, in the Gulf Stream system. The division of a cyclone into two vortices in the Bermuda Islands region, described by Cheney *et al.* (1976), was observed in September–December 1974 by SOFAR acoustic floats. Richardson, Maillard & Stanford (1979) described the decay of the elliptical 'Allen' vortex into two cyclones moving in opposite directions. Kennelly, Evans & Joyce (1985), when analysing the so-called '82B' anticyclonic vortex, provided information on the cyclonic vortex-satellites found at its periphery, referring to them as 'ringlets'. They suggested that anticyclonic vortex instability might be a cause of ringlet generation.

The theoretical study of the axially symmetric two-layer heton performed by Kozlov, Makarov & Sokolovskiy (1986, referred to hereinafter as KMS), found that at $\gamma > 1.7$ (see Appendix A) the vortex structure can be unstable with respect to small disturbances in shape. Vortex stability was studied in more detail by Helfrich & Send (1988). Sokolovskiy (1988) examined the stability of ring-shaped or shielded two-layer vortex structures, looking at the formation of the cyclonic ringlet series at the periphery of the anticyclonic core of the vortex. Carton & Corréard (1997) also studied the stability of a two-layer vortex and identified the conditions for the formation of a two-layer analogue of the tripolar structure.

The tendency of close, like-sign vorticity patches to merge is another characteristic feature of finite-core vortices. There are known cases of vortex merging in the ocean. Thus, Cresswell (1982) described the results of 20 days of observations of a large new warm vortex formed by the merging of two vortices, 'Mario' and 'Leo', which were separated from the East-Australian Current in early 1981. Robinson *et al.* (1986) provided a detailed description of the merging of two anticyclones in the California Current System during the 1983 OPTOMA-V experiment. Laboratory modelling of the merging of two-layer vortices was carried out by Griffiths & Hopfinger (1986, 1987) and Nof & Simon (1987), for example. The first study by Griffiths & Hopfinger describes the results of the interaction between two hetons when the vortex patches are located in different layers. In their second study, they examined the dependence of the deformation radius on the critical distance at which the vortex patches of the same sign in the upper layer merge. Nof & Simon (1987) investigated the merging process for baroclinic vortices with the same density and slightly different densities.

A number of studies have examined the different theoretical aspects of the merging of the finite-core baroclinic vortices. Calculations based on the pseudo-spectral finite-difference method (Verron, Hopfinger & McWilliams 1990; Verron & Hopfinger 1991; Valcke & Verron 1993, 1996, 1997; Verron & Valcke 1994) have shown that different types of connected vortex structures may appear, depending on stratification. They also discuss the question of vorticity initialization, which is important when interpreting the results of laboratory experiments, such as those carried out by Griffiths & Hopfinger (1987). The two-layer generalization of the contour dynamics method

(CDM) was used by Polvani, Zabusky & Flierl (1989) to study the merging and formation of new quasi-stationary states (V-states) following interaction between two vortex patches localized in the upper layer. Polvani (1991) found new V-states for two-layer vortices and in particular for hetons. The analogous two-layer CDM version was used by Sokolovskiy (1989; 1990*a*, *b*) to study some cases of interaction between two hetons.

In concluding this overview, it is worth mentioning the review papers by Gryanik (1990) and Hopfinger & van Heijst (1993) which provide detailed analysis of the stability, division and merging of both barotropic and baroclinic vortices.

The objective of the present paper is to provide a general view of possible interactions (and certain stability properties) between two-layer baroclinic eddies and especially hetons. One goal is to examine several of the configurations which have been studied in isolation in an attempt to determine controlling parameters, i.e. the initial geometry and especially the vertical alignment of the vortex patches, and stratification. Section 2 presents the results for an isolated two-layer vortex structure when the two vortex patches in the different layers are (i) vertically aligned, (ii) tilted on the vertical. In § 3, the general case of two two-layer vortices is examined. Again, the case of two vertically aligned two-layer vortices is considered first. This assumption is then relaxed for one of the vortices, so that one two-layer vortex is vertically aligned and the other tilted. Finally, the two two-layer vortices are assumed to be vertically tilted.

The theoretical basis is the classical quasi-geostrophic (QG) model for a two-layer ocean (e.g. Pedlosky 1987; Ikeda 1981; Cushman-Roisin, Sutyrin & Tang 1992) on the $f$-plane, with a 'rigid lid' at the surface, a flat bottom and layers of equal thickness. Two types of eddy model are considered:

(i) Single-point vortices (Gryanik 1983; Hogg & Stommel 1985*a*, *b*). In this case, analytical equations can be written. Vortex intensity is denoted by $s$.

(ii) Finite-core vortices with constant values of PV. The CDM is then used (KMS; Helfrich & Send 1988; Polvani *et al.* 1988, 1989). (Note that some further information on the application of CDM is given in Appendix B.) Potential vorticity is denoted by $\Pi$.

Synoptic scale vortex movements which are described adequately by QG theory must have a horizontal characteristic scale of the same order as the radius of deformation (Kamenkovich, Koshlyakov & Monin 1986). In this work, parameters are chosen to satisfy this constraint which is actually written as $\gamma = O(1)$. In all subsequent calculations, the initial location of vortices is as indicated in figure 1 for a single two-layer vortex (figure 1*a*) and two two-layer vortices (figure 1*b*). As can be seen in the figures, cases of symmetrical vortices with respect to the $y$-axis are considered. Here, and in most subsequent figures, the contours of upper-layer vortices are drawn with a solid line and those of lower-layer vortices with a dashed line. The upper number defines the reference number of the two-layer vortex (two-layer vortex 1 or two-layer vortex 2) and the lower number indicates the number of the layer (upper layer 1 or lower layer 2). For example, $s_2^1$ and $\Pi_2^1$ represent the vortex intensity and the PV of the lower layer of vortex 1, respectively, in a point-vortex configuration and in a finite-core configuration. Vortex centres of the upper and lower layers are represented, respectively, by circles and boxes. In the case of two hetons, the markers for the first are solid, and those for the second are empty. In all calculations, upper-layer vortices are anticyclonic, while those of the lower layer are cyclonic. Thus, the corresponding hetons are warm (Hogg & Stommel 1985*a*). $B$ has a positive value, and $D, D_1$ and $D_2 \geqslant 0$. When $D = D_1 = D_2 = 0$, the two-layer vortices have vertical axes as in classical cases (Gryanik & Tevs 1989; Polvani 1991). For non-zero values of any of these parameters, the axes are tilted.

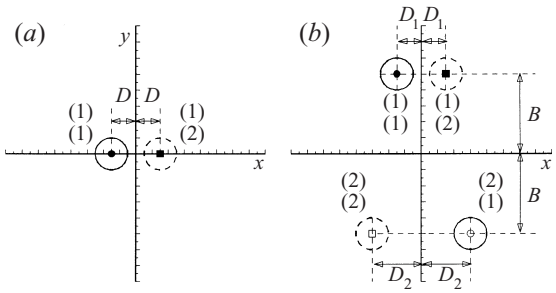


FIGURE 1. Diagram of initial vortex position: (*a*) one heton; (*b*) two hetons.

## 2. A single two-layer vortex structure

### 2.1. *Vertically aligned vortex patches* ($D = 0$)

Let the potential vorticities $\Pi_1^1$ and $\Pi_2^1$ be non-zero only in domains $S_1^1$ and $S_2^1$ (see also Appendix B), which are initially circles of unit radius (without loss of generalities, similar assumptions on the initial shapes and sizes of the vortex patches are made in all experiments), as their centres are placed at the origin of the coordinates. We are therefore examining the case of a two-layer vortex structure which initially consists of two circular vorticity patches located in the upper and lower layers. When a structure is thus axisymmetric and $\Pi_1^1 = -\Pi_2^1$, azimuthal velocities in both layers can be found, according to KMS, using the formula

$$V_i(r) = \Pi_i^1 \begin{cases} K_1(\gamma)I_1(\gamma r) & \text{if } r < 1, \\ I_1(\gamma)K_1(\gamma r), & \text{if } r \geqslant 1, \end{cases} \tag{1}$$

where $I_1(x)$ and $K_1(x)$ are modified Bessel functions. This is a purely baroclinic distribution of azimuthal velocity with rotation in opposite directions in different layers, which is appropriate to a heton.

Below, many of the figures represent instantaneous positions of the vortex patch contours at given times. In every experiment, jumps of potential vorticity $\Pi_i^j$ have been chosen such that the unit timescale is equal to the rotational period of the fluid particle moving along the contour of the initial patch.

In the case of discrete vortices, when the contours $C_1^1$ and $C_2^1$ shrink to a point, the expressions for the azimuthal velocity radial distribution have the following form:

$$V_i(r) = \frac{\gamma s_i^1 K_1(\gamma r)}{2\pi}, \quad i = 1, 2. \tag{2}$$

As previously stated, $s_i^j$ denotes the intensity of point vortices, analogous to potential vorticity $\Pi_i^j$. The results of calculations made for both finite-core vortices and point vortices will be discussed below. We selected the intensity of the discrete vortex $s_i^j$ from the condition of 'equivalence' (Polvani 1991) such that the azimuthal velocity along the imaginary unit circle induced by this vortex is equal to the velocity along the contour of the finite-core vortex of the same radius. These considerations allow us to assign the same meaning to the parameter in both cases of discrete and finite-core vortices. From (1) and (2) we obtain:

$$(s_i^1)_{eq} = \frac{2\pi\Pi_i^1 I_1(\gamma)}{\gamma}, \quad i = 1, 2. \tag{3}$$

Note that any axially symmetric distribution of the potential vorticity defines some

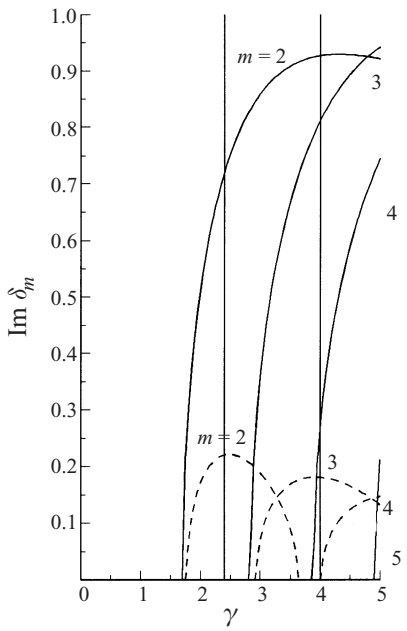


FIGURE 2. Growth rate dependencies of first unstable modes $\mathrm{Im}\delta_m$ on the parameter $\gamma$. ——, a compensated two-layer vortex-heton ($\xi = -1$); – – –, a non-compensated two-layer vortex ($\xi = -0.25$). Vertical solid lines correspond to values $\gamma = 2.4$ and $\gamma = 4$. Numerical calculations given in figures 3 and 4 were made using these values of $\gamma$.

stationary state. This is also valid for the distribution considered now. The problem of vortex stability with respect to small azimuthal disturbances of the shape (for the more general case of arbitrary $h_1$ and $h_2$) is exposed in KMS. We will now examine this approach in more detail. Let the fluid lines delimiting the constant potential vorticity area be described by parametric relations as follows:

$$r = f_i(\theta, t; \alpha), \quad \alpha = f_i(\theta, 0; \alpha), \quad i = 1, 2$$

where the parameter $\alpha$ characterizes the radial Lagrange coordinate of the points belonging to the contours, and $\theta$ is the polar angle. Thus, we can write:

$$f_i(\theta, t; \alpha) = \alpha + \epsilon_i(\alpha) \exp\left[im(\theta - \delta_m t)\right], \quad |\epsilon_i| \ll \alpha, \quad i = 1, 2, \quad m \geqslant 1 \tag{4}$$

where $m$ is the number of the azimuthal mode. Naturally, the condition $\mathrm{Im}\delta_m > 0$ ($\mathrm{Im}\delta_m$ is the imaginary part of $\delta_m$) should be fulfilled for unstable modes. The problem reduces to the solution of the system of algebraic linear equations with respect to $\epsilon_i$. In particular, in KMS, it was established that:

(i) the necessary condition for instability is the change in sign of potential vorticity ($\Pi_1^1 \Pi_2^1 < 0$);

(ii) at $m = 1$, the instability condition cannot be fulfilled. When $m \geqslant 2$, it is possible to identify the areas of instability. For example, in the plane of the parameters $(h_1, \gamma)$, stability is less when $m = 2$. In the present case, where $h_1 = h_2 = 0.5$, vortex instability exists when $\gamma > 1.7$.

Figure 2 shows the growth rates for unstable modes $m = 2, 3, 4$ depending on the parameter $\gamma$. The quantity $\mathrm{Im}\delta_m$ characterizes the degree of instability of the mode $m$. Two specific cases are considered: $\xi = -1$ and $\xi = -0.25$, where $\xi = \Pi_2^1 / \Pi_1^1$. In the first case, the 'compensated' two-layer vortex (heton) is obtained, whereas in the

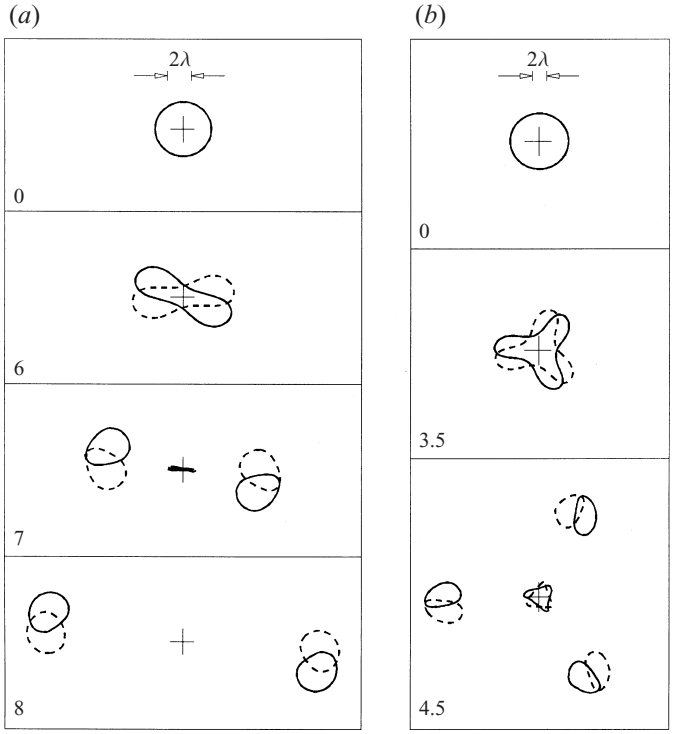


FIGURE 3. Evolution of an unstable heton ($\xi = -1$): (*a*) $\gamma = 2.4$; (*b*) $\gamma = 4$. Here and in the following figures, the cross denotes the position of the origin of the coordinate system and numbers are the values of the non-dimensional time.

second case the cyclonic vortex of the lower layer is four times less intense than the upper layer anticyclone. Here, and in all other figures showing contours of the vortex patches, dimensionless time is shown in the bottom left-hand corner and the cross indicates the origin of the coordinate system $(x, y)$.

Figure 3 demonstrates the decay process for an unstable two-layer vortex which is initially axially symmetric at the given values of $\gamma$. Figure 3(*a*) illustrates the development of an unstable mode with $m = 2$. In this case, each layer vortex patch keeps a fairly circular shape for some time. It then becomes deformed and acquires a quasi-elliptic configuration. Finally, it breaks into two parts. As a result of this process, two hetons with tilted axes appear and then move away in opposite directions. Figure 3(*b*) shows the domain of the unstable second, third and fourth modes and, despite the fact that $\mathrm{Im}\delta_2 > \mathrm{Im}\delta_3$, we can see the structure of the mode with $m = 3$. Here, the collapse of the circular heton results in the formation of a central quasi-triangular two-layer structure and three hetons with tilted axes that move away from this structure at an angle of 120°.

A non-compensated two-layer vortex (figure 4) evolves quite differently. Thus, in figure 4(*a*) we see the formation of a two-layer analogue of a tripolar structure from the axially symmetric vortex. The anticyclonic vortex patch of the upper layer takes on a pulsating quasi-elliptic shape, and the cyclone of the lower layer collapses and, by getting rid of small vortex threads, forms two vortices close to the circular vortices. The entire configuration rotates clockwise. Calculations conducted over a longer time period than that shown in the figure suggest that such a structure is stable. This is

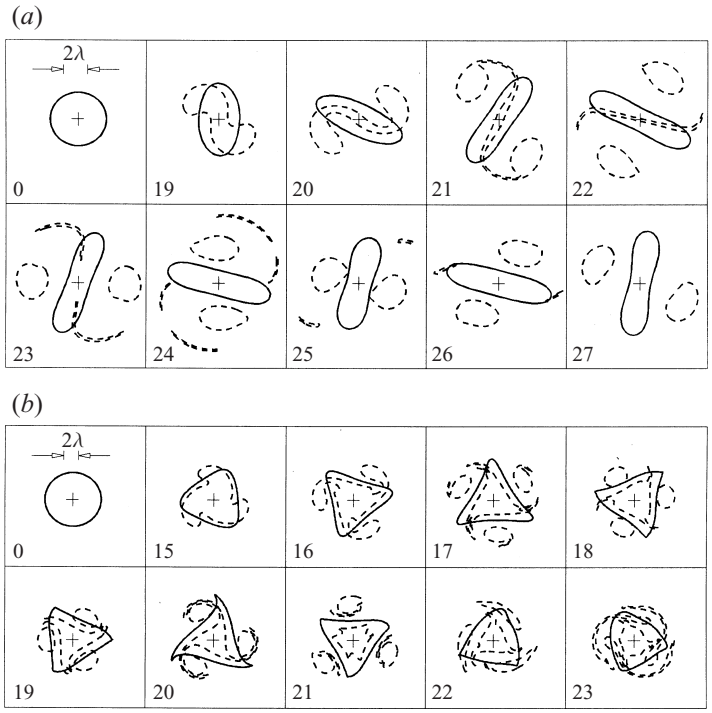


FIGURE 4. Evolution of an unstable two-layer vortex with a barotropic component ($\xi = -0.25$): (*a*) $\gamma = 2.4$; (*b*) $\gamma = 4$.

in agreement with Carton & Corréard (1997). In contrast, figure 4(*b*), which shows the formation of a two-layer quadrupole structure, clearly characterizes unstable behaviour, which is perhaps why Carton & Corréard (1997) were not able to identify it. The formation of configurations analogous to those in figures 3 and 4 was studied by Helfrich & Send (1988) and Corréard & Carton (1997). Earlier, the formation of two-layer tripolar structures had been identified by Ikeda (1981). Baroclinic tripolar structures resulting from the collapse of a two-layer vortex, submerged into a shear flow, have also been observed by Yano & Flierl (1992). Configurations qualitatively close to those mentioned above were obtained by Sokolovskiy (1997*a*, *b*) for a three-layer model. Sokolovskiy called such vortex structures 'roundabout' structures, as they consist of a rotating structure, followed by smaller disks attached below and connected to it by swivels. These disks are also able to rotate around their instantaneous axes.

Note that there exists an analogy between a two-layer vortex consisting of two axially symmetric circular vortex patches rotating in opposite directions in the layers and a barotropic ring-shaped vortex, the core and surrounding cover of which have opposite signs – a shielded vortex (Kozlov & Makarov 1985; Morel & Carton 1994; Makarov 1996; Valcke & Verron 1997). In the case of complete compensation, such a vortex (where the ratio between the radii of the core and the whole vortex is greater than 0.5) becomes unstable and breaks into two or more dipoles (an analogous case to that in figure 4). When compensation is absent, the vortex can form tripolar, quadrupolar and generally multipolar structures (analogous to figure 4) as shown by Makarov (1996).

It is worthwhile emphasizing in this section that the two-layer vortex with a vertical axis is neutrally stable when $\gamma \leqslant 1.7$; in this case, it stays motionless as a whole and

the circular shape of its vortex patches remains practically unchanged. When $\gamma > 1.7$, the vortex becomes unstable and breaks down into baroclinic vortex structures of smaller scale. Naturally, the theoretical analysis of the stability of a vortex with a tilted axis is much more complicated. The numerical simulations presented in the next section contribute to a better understanding of this.

### 2.2. *Tilted axis vortex structures* ($D \neq 0$)

#### 2.2.1. *Discrete vortices*

Let two discrete vortices in the upper and lower layers with respective coordinates of $(x_1, y_1)$ and $(x_2, y_2)$ be placed at some distance $r = \sqrt{(x_2 - x_1)^2 + (y_2 - y_1)^2}$ from each other and have intensities of $s_1^1$ and $s_2^1$. If the vortex system is a dipole of vortices (i.e. $s_1^1 = -s_2^1$), then the vortices move rectilinearly at constant velocity (Hogg & Stommel 1985*a*)

$$V = \frac{s_1^1}{4\pi r}[1 - \gamma r K_1(\gamma r)]. \tag{5}$$

The main properties of point vortex interaction in the two-layer medium may be stated as follows:

(i) If two vortices are located in different layers, the dependence of their velocity on distance has a non-monotonous character. The velocity vanishes both when $r \to 0$ and when $r \to \infty$. In particular, this allows the vortices to approach each other, coalesce and exchange locations. The velocity of two vortices belonging to the same layer is a monotonous function of the distance between them and becomes infinite when $r \to 0$ (see also Appendix A).

(ii) Analysis of vortex interaction energy (Gryanik 1983) leads to the conclusion that interaction has a rather barotropic character if the distances between the vortices significantly exceed the radius of deformation. When these distances become smaller, the role of baroclinic interaction increases. Owing to this fundamental property, it is possible to reach a conclusion which has been confirmed by numerous calculations (Gryanik 1983; Hogg & Stommel 1985*a*, *b*; Gryanik & Tevs 1989, 1997): at distances smaller than $\lambda$, interaction between vortices of the same layer plays the main role; at distances greater than $\lambda$, interaction between the eddies of different layers is marked.

(iii) In both limiting situations when $\gamma \to \infty$ and $\gamma \to 0$ (i.e. respectively, $\lambda \to 0$ and $\lambda \to \infty$), the two-layer stratified fluid behaves as a barotropic fluid. In the first case, the densities of the fluid in the upper and lower layers become the same. In the second case, interaction between the layers becomes impossible because of the theoretically infinite density jump at their interface. In light of this observation, properties (i) and (ii) actually stand for $\gamma = O(1)$.

We will show that these properties are also valid when finite-core vortex patches interact.

#### 2.2.2. *Finite-core vortices*

Let two vortex patches be located in different layers and not vertically aligned with one another, i.e. the vortex has a tilted axis. As before, we will assume that the boundaries of the vortex patches are circles at the initial instant. It is certain that such a circular shape does not correspond to a steady state (Polvani 1991), but as the vortex patches develop they evolve towards the appropriate shape. This can be seen in figure 5(*b*).

Let us now discuss the simulation results. These are related primarily to the stability of such two-layer vortices with tilted axes. Naturally, in the range of parameters for

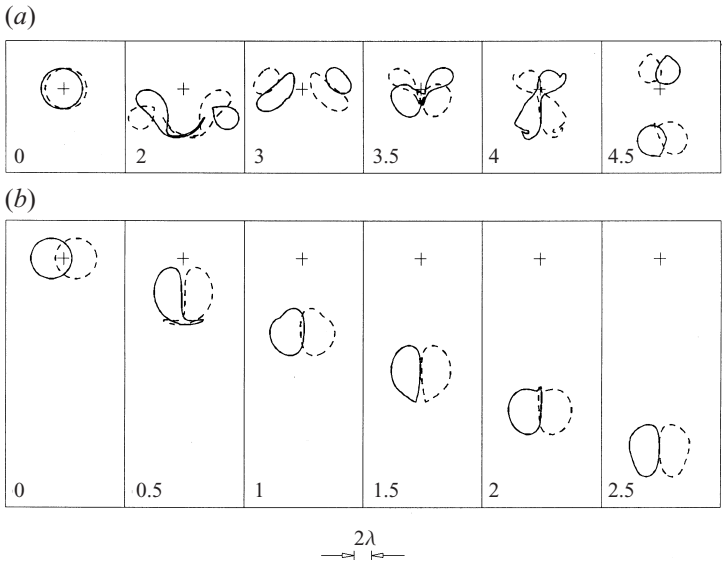


FIGURE 5. Evolution of a heton with tilted axis at $\gamma = 2.4$: (*a*) $D = 0.1$; (*b*) $D = 0.6$. Black circles from figure 6 correspond to these experiments.

which the axially symmetric two-layer vortex is stable, the inclination of its axis results only in the initiation of the heton's translational movement. Such a stable translational state was studied in detail by Polvani (1991). If $\gamma > 1.7$ and then the axially symmetric vortex is unstable, the potential ability of the vortex structure to collapse will influence the behaviour of the vortex with the tilted axis. Figure 5(*a*) confirms that such vortex collapses can occur at relatively small angles of axis inclination. Here, the heton (under the effect of the dipole) starts to move and, at the same time, collapses. All the vortex patches break into two unequal parts and form two non-compensated two-layer vortices. These rotate around their tilted axes and when two patches come close enough to each other, they merge temporarily in each layer, then break down and recombine. As a result, two new hetons with tilted axes are generated, which then move away in opposite directions. The final stage of the process resembles that shown in figure 3(*a*). However, there is a distinctive feature. In the case of an axially symmetric vortex, the newly formed dipoles diverge in arbitrary directions, whereas here it is predetermined by the initial configuration. When the dipoles are not equivalent, the most powerful heton moves in the same direction as that of the initial vortex, while the less powerful heton moves in the opposite direction.

In fact, setting a non-zero value for parameter $D$ interprets the role of the initial perturbation of the vortex shape. As every vortex patch is always stable in itself, we might expect that the interaction of the vortex patches which are sufficiently distant from one another will not destroy the heton. The calculations give an unexpected result: as soon as $D > 0.5$, when the patches still significantly overlap, the hetons become stable irrespective of the value of the deformation radius. Figure 5(*b*), in which the configurations at different times are superimposed, confirms this conclusion.

The diagram showing the distribution of stable and unstable states of finite-core hetons with tilted axes in the $(\gamma, D)$-plane is given in figure 6. It should be noted that in this figure, and in all other similar figures (figures 8, 11, 15), the boundaries separating different regimes have been based on the calculations using 0.1 steps along

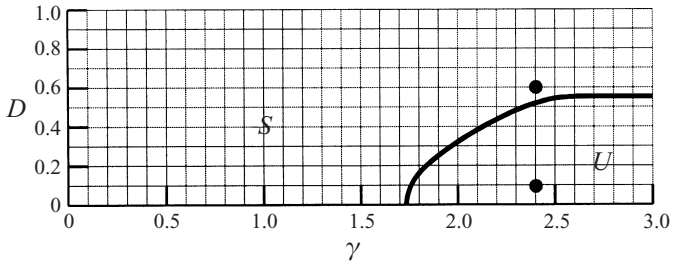


FIGURE 6. Diagram in the $(\gamma, D)$-plane ($0.1 \leqslant \gamma \leqslant 3, \quad 0 \leqslant D \leqslant 1$) of stable ($S$) and unstable ($U$) states of finite-core hetons with tilted axis ($D \geqslant 0$).

both coordinate axes. As with unique discrete hetons, the movement of finite-core hetons is uniform and rectilinear, irrespective of the deformation radius.

## 3. Two two-layer vortices

Let us examine different kinds of interaction between two hetons with both discrete and finite cores, with an initial location as shown in figure 1($b$). Based on the previous assumptions, the equations for the movement of contour nodes for vortex patches (see Appendix B, equation (B 1)) are solved now at $J_1 = J_2 = 2$, and the movement of singular vortices is governed by the following relations:

$$\frac{\mathrm{d}x_i^j}{\mathrm{d}t} = -\frac{1}{4\pi}\left\{ s_i^{3-j}\frac{y_i^j - y_i^{3-j}}{(r_{ii}^{j(3-j)})^2}[1 + \gamma r_{ii}^{j(3-j)} K_1(\gamma r_{ii}^{j(3-j)})] + \sum_{n=1}^{2} s_{3-i}^n \frac{y_i^j - y_{3-i}^n}{(r_{i(3-i)}^{jn})^2}[1 - \gamma r_{i(3-i)}^{jn} K_1(\gamma r_{i(3-i)}^{jn})] \right\}, \tag{6}$$

$$\frac{\mathrm{d}y_i^j}{\mathrm{d}t} = \frac{1}{4\pi}\left\{ s_i^{3-j}\frac{x_i^j - x_i^{3-j}}{(r_{ii}^{j(3-j)})^2}[1 + \gamma r_{ii}^{j(3-j)} K_1(\gamma r_{ii}^{j(3-j)})] + \sum_{n=1}^{2} s_{3-i}^n \frac{x_i^j - x_{3-i}^n}{(r_{i(3-i)}^{jn})^2}[1 - \gamma r_{i(3-i)}^{jn} K_1(\gamma r_{i(3-i)}^{jn})] \right\}, \tag{7}$$

where $i = 1, 2$, $j = 1, 2$ and $r_{ij}^{mn} = \sqrt{(x_j^n - x_i^m)^2 + (y_j^n - y_i^m)^2}$ is the distance between vortex $n$ of layer $j$ and vortex $m$ of layer $i$. In this case, the initial conditions take the form:

$$x_1^1 = -x_2^1 = -D_1, \quad x_1^2 = -x_2^2 = D_2, \tag{8}$$

$$y_1^1 = y_2^1 = -y_1^2 = -y_2^2 = B. \tag{9}$$

Equations (6) and (7) with initial conditions (8) and (9) were solved using the standard second order of the Runge–Kutta method and a timestep $\Delta t = 0.01$. Similar problems have been discussed in the studies by Gryanik (1983) and Hogg & Stommel (1985$a$, $b$). Figure 9 from Hogg & Stommel (1985$a$) contains comprehensive information on the movement of point vortices at their initial position, represented in figure 1($b$) as $D_1 = D_2 \equiv D$. The interaction of finite-core hetons at $D = 0$ was studied by Valcke & Verron (1993, 1996, 1997) and Verron & Valcke (1994). Presented below

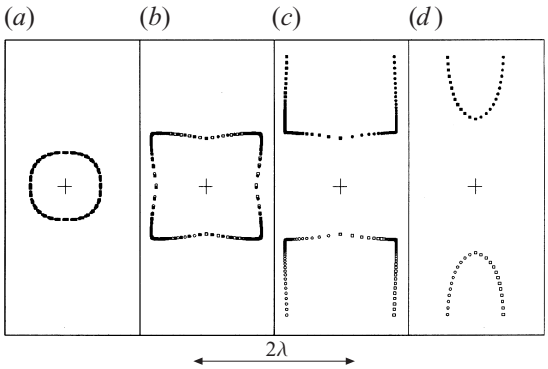


FIGURE 7. Trajectories of movement of two discrete hetons at $\gamma = 0.5$ and $D = 0$: (*a*) $B = 1$; (*b*) $B = 1.433$; (*c*) $B = 1.434$; (*d*) $B = 2$. Black boxes from figure 8 correspond to these experiments.

are the results of a more general examination of the interaction of two hetons taking into account these previous studies.

### 3.1. *Two hetons with vertical axes* ($D_1 = D_2 = D = 0$)

#### 3.1.1. *Discrete vortices*

Based on Hogg & Stommel (1985*a*), there are two possible types of movement when two discrete hetons are located initially on the $y$-axis:

(i) where $B\gamma > (B\gamma)^* \approx 0.7165$, the vortices in the upper and lower layers of each heton slide apart. This means that the axes of the hetons become tilted and they scatter in opposite directions. It is clear that, in this situation, interaction within each heton is predominant.

(ii) where $B\gamma < (B\gamma)^*$, the vortices in the upper (lower) layer rotate in an anticyclonic (cyclonic) direction along the O-shaped overlapping orbits. In this situation, interaction occurs mainly between the vortices located in each layer.

The existence of these two types of movement tends to confirm conclusion (ii) of § 2.2.1.

Figure 7 illustrates these points. Note that close trajectories, similar to those shown in the two sketches on the left-hand side of this figure, have the following peculiarities. Where $B\gamma \to 0$, the trajectories 'try' to have a circular shape and the angular velocity of vortex movement tends to a constant value. Where $B\gamma \to (B\gamma)^*$, the trajectories take the shape of a deformed square, its angular points becoming bifurcation points. It is obvious that each angular point corresponds to an unstable (saddle) stationary state. Thus, it can be seen that the two types of movement in the $(\gamma, B)$-plane are divided by the hyperbola

$$B\gamma = (B\gamma)^*. \tag{10}$$

#### 3.1.2. *Finite-core vortices*

In Valcke & Verron (1993), the interaction of two vortices with finite cores and vertical axes was examined. The authors based their calculations on the pseudo-spectral method and took into account a small level of biharmonic friction that allowed them to classify heton interaction according to two parameters: the distance between their centres ($2B$ in the calculations) and the relative radius of deformation $\lambda/R = \gamma^{-1}$. In the plane of these variables, they identified three types of interaction: besides types (i) and (ii) mentioned above, which are appropriate to point vortices,

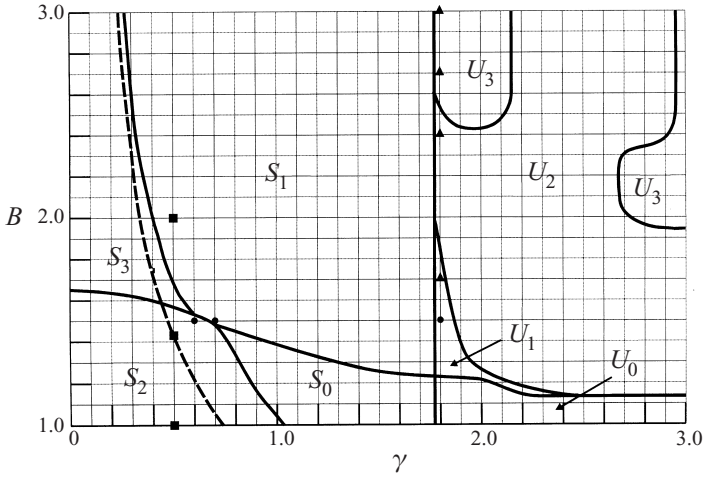


FIGURE 8. Diagram in the $(\gamma, B)$-plane ($0.1 \leqslant \gamma \leqslant 3; 1 \leqslant B \leqslant 3$) of the states of the system consisting of two finite-core hetons at $D = 0$. Regions are denoted as follows: $S_1$, scattering of hetons in opposite directions along the straight line passing through their centres in the initial state; $S_0$, the same but after merging of vortex patches and their subsequent division; $S_2$, merging of vortex patches into quasi-elliptical vortex structures in the layers; $S_3$, layerwise rotation of vortex patches in opposite directions without merging; $U_0$, merging of the hetons followed by their subsequent division into more than two smaller hetons, which then scatter; $U_1$, reciprocal moving away of initial hetons without merging, followed by their subsequent breaking down into four newly formed dipoles; $U_2$, breaking down of the hetons into non-compensated vortices followed by the merging of vortex patches and formation of new hetons; $U_3$, breaking down of the hetons into scattering two-layer vortices without subsequent merging. The dashed line (corresponding to equation (10) in the text) separates the areas of finite and infinite solutions in the theory of discrete vortices. The meaning of the markers is explained in the captions for figures 7, 9 and 10.

they also determined the class of movement, when patches with the same vorticity merge in the layers, forming a connected state. Type (i) movement was referred to in Valcke & Verron (1993) as 'heton interaction'. The authors noted an interesting property of two-layer vortices in that they scattered even when, in the initial stages of movement, the vortex patches in each layer belonging to different hetons merged. They identified the area of diverging movement as Region 1, the area of vortex merging as Region 2, and the area of rotation without merging as Region 3.

In this paper, we will study heton interaction in detail using the CDM. Legras & Dritschel (1993), in a study comparing pseudo-spectral and CDM methods, approximated the continuous distribution of vorticity by a multi-step function comprising 8 and 16 levels. The comparison gives very close quantitative results. The authors note that CDM is more convenient when studying the processes of filamentation, merging and vortex division. In this paper, a crude approximation is used by replacing the continuous Gaussian distribution of vorticity in Valcke & Verron (1993) by a one-step function.

A summary of all these results is plotted in the $(\gamma, B)$-plane and shown in figure 8. The choice of the coordinate $\gamma$ instead of $\gamma^{-1}$ was made for the sake of convenience, as only a narrow interval of small values of $\gamma^{-1}$ corresponds to the hetonic class of movement.

It is important to note that although friction is not taken into account in our model (in fact, contour surgery removes the smaller filaments) and, as mentioned above, the CDM is approximate, the boundaries between the regions in Valcke & Verron (1993)

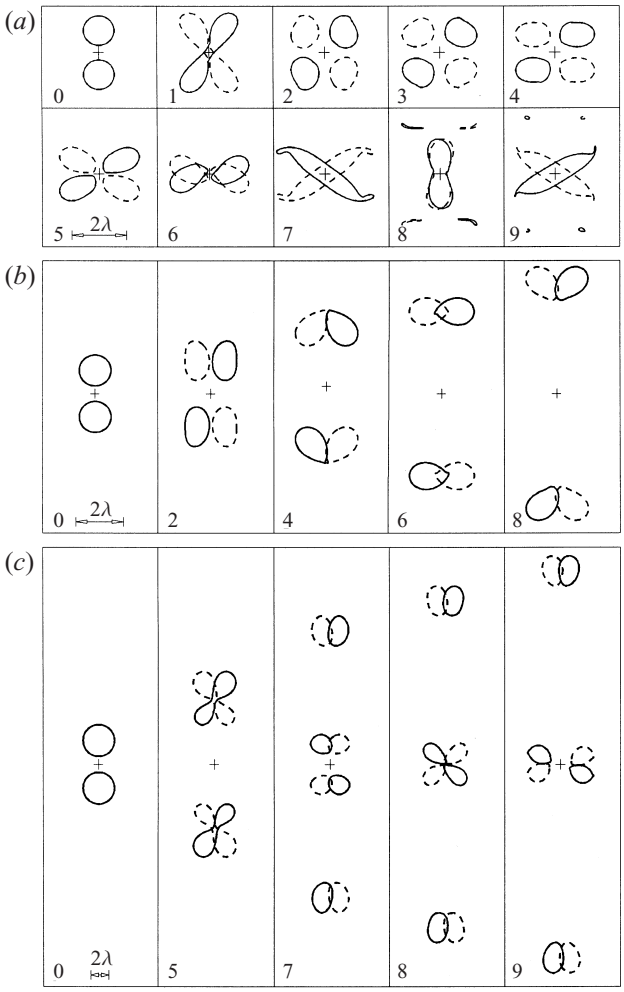


FIGURE 9. Evolution of two hetons with vertical axes ($D = 0$) at $B = 1.5$: (*a*) $\gamma = 0.6$; (*b*) $\gamma = 0.7$; (*c*) $\gamma = 1.8$ (black circles in figure 8).

coincide practically everywhere with those in the present study, except for the interval $0.5 < \gamma < 1$. Thus, in figure 8, $S_2$ corresponds to Region 2, $S_3$ to Region 3, and all others to Region 1. In the following paragraphs, the peculiarities of Region 1 will be studied in detail. The dashed line corresponding to the limit given by equation (10), which is the boundary dividing the areas of type (i) and type (ii) vortices, shows that finite-core vortices behave like point vortices from the point of view of interaction where $\gamma \leqslant 1.7$ and $B \geqslant 1.7$. The results of our CDM calculations, as shown in figure 8, are discussed in more detail below.

Figure 9 shows a sequence of interactions between two hetons with vertical axes at the initial instant, for $B = 1.5$. According to figure 9(*a*), when $\gamma = 0.6$, vortex patches rotate in every layer; they merge, divide, then merge again, throwing off small vortex structures. We did not observe further divisions (the calculations were made up to $t = 20$), i.e. a type $S_2$ connected structure is formed. When $\gamma = 0.7$ (figure 9*b*), the hetons, having acquired tilted axes, move in opposite directions without intermediate merging (type $S_0$). In figure 9(*c*), when $\gamma = 1.8$, the hetons begin to drift away and, in

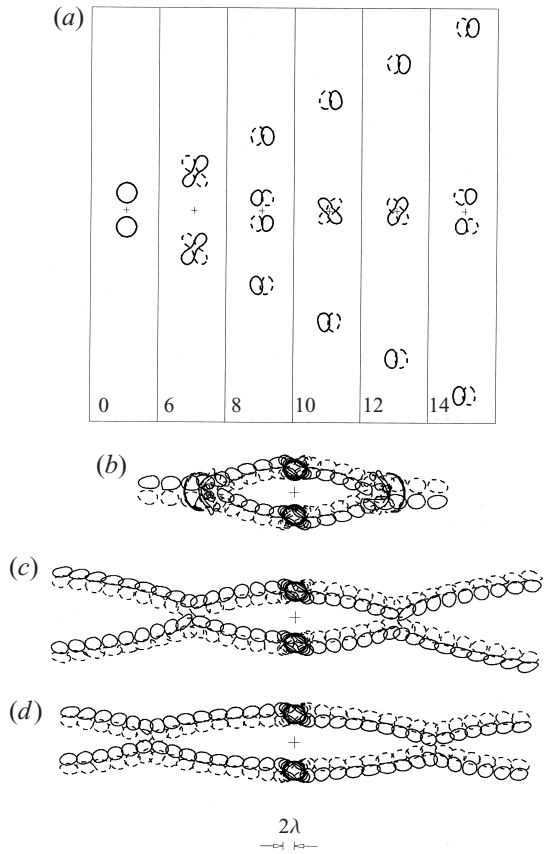


FIGURE 10. Evolution of two hetons with vertical axes at $\gamma = 1.8$: (*a*) $B = 1.7$; (*b*) $B = 2.4$; $t = 0, 1, \ldots, 13$; (*c*) $B = 2.7$; $t = 0, 1, \ldots, 19$; (*d*) $B = 3$; $t = 0, 1, \ldots, 19$ (black triangles in figure 8).

so doing, collapse because of instability, dividing into two two-layer unequal dipoles which then move away in opposite directions. As a result, smaller heton dipoles, which have collided with one another, exchange partners and newly formed hetons move in a perpendicular direction (type $U_1$). Larger dipoles still move in opposite directions along the $y$-axis.

Figures 9(*a*) to 9(*c*) thus demonstrate a sequence of transitions between different classes of movement with a constant initial distance, $B$, between the hetons and the radius of deformation.

Figure 10 shows the influence of varying distance $B$ at a constant value $\gamma$; here, $\gamma = 1.8$ was chosen. An interesting solution is shown in figure 10(*a*), where $B = 1.7$. Here, after the collapse of the hetons, their head sections drift away along the $y$-axis, and vortex patches relating to the tail parts move towards each other, merge, start rotating in opposite directions, then divide again into two hetons with tilted axes, which chase after the head sections. In this way, the two-layer dipoles then collide, with an inelastic impact.

Note that numerical experiments, illustrated in figures 9(*c*) and 10(*a*), were conducted at $B = 1.5$ and $B = 1.7$, respectively, all other parameters being equal. They give qualitatively different results after the short phase during which the vortex

patches of small hetons merge. Thus, in the first case, we observe the divergence of divided two-layer dipoles along the $x$-axis, and in the second case, along the $y$-axis.

Let us attempt to explain this effect. In figure 9($c$), at the initial instant, the centres of the hetons are closer to one another than in figure 10($a$). Consequently, heton interaction is at its strongest in figure 9($c$). So that on the one hand the hetonic mechanism of reciprocal pushing away has a maximum effect and, on the other, the hetons begin to collapse earlier. At the last moment, just before the vortex patches merge, the respective values obtained for their centres were $x = \pm 0.69$ and $x = \pm 0.60$. It was found that such small differences are sufficient for the decay of the central connected structure to occur earlier in the first case than in the second. In spite of these qualitative differences, both cases can be related to the same type of interaction ($U_1$): reciprocal moving away of initial hetons without merging, followed by a breakdown into four newly formed dipoles.

Figures 10($b$), 10($c$) and 10($d$) show the general pattern of movement when $B = 2.4, 2.7$ and 3, respectively. In the first case, heton interaction belongs to type $U_2$ movement with an intermediate stage of heton structuring following the merging of the non-compensated two-layer vortices. In the second and third cases, movement is of the $U_3$ type. Here, we have shown the initial stage of the process, when the two-layer vortices of smaller scale periodically experience lateral collision, with subsequent scattering. It is clear that the period is related to the initial distance $B$ between the hetons (seen in the comparison of figures 10($c$) and 10($d$)).

Thus, figures 9 and 10 provide some typical examples of interaction between finite-core hetons which initially have vertical axes. In particular, they show that it is convenient to divide the class of 'heton interaction' into subclasses with qualitatively different kinds of movement.

### 3.2. *One vortex with a vertical axis and one vortex with a tilted axis* ($D_1 = 0, D_2 > 0$)

Since a vortex with a vertical axis is motionless as a whole, and the translational velocity of a vortex with a tilted axis is not equal to zero, we can consider the effect of a two-layer dipole on a motionless heton. In this subsection, the amplitude of the inclination of the incident heton is a free parameter, and only two cases are discussed in relation to distance $B : B = 1.5$ and $B = 2.5$.

#### 3.2.1. *Discrete vortices*

Based on the previous section, it can be seen that only two kinds of discrete vortex movement are possible when $D_2 = 0$: anticyclonic rotation in the upper layer and cyclonic rotation in the lower one, or heton scattering in opposite directions when $D_2 > 0$. Results of the calculations are summarized in figure 11(i). Essentially, three kinds of movement are possible, depending on external parameters. The prototype of rotational movement appears to be the two-layer analogue of the so-called 'vortex game' (type 3), when each dipole performs simultaneous translational and rotational movements. An example of this type of heton interaction is shown in figure 12($a$). Heton scattering when $D_2 > 0$ also has its specific features. In the first stage of movement, the inclination of the axis of the incident heton gradually decreases, vanishes and finally changes its sign. In doing so, its velocity decreases and passes through a zero value (but this takes place after the inclination of the axis has changed signs). Then the hetons change their direction of movement (type 1). During this stage, axis inclination and the velocity of translational movement of the initially motionless heton continue to increase. In the second stage, the hetons with constant velocity move away in opposite directions. It is clear that during this process the

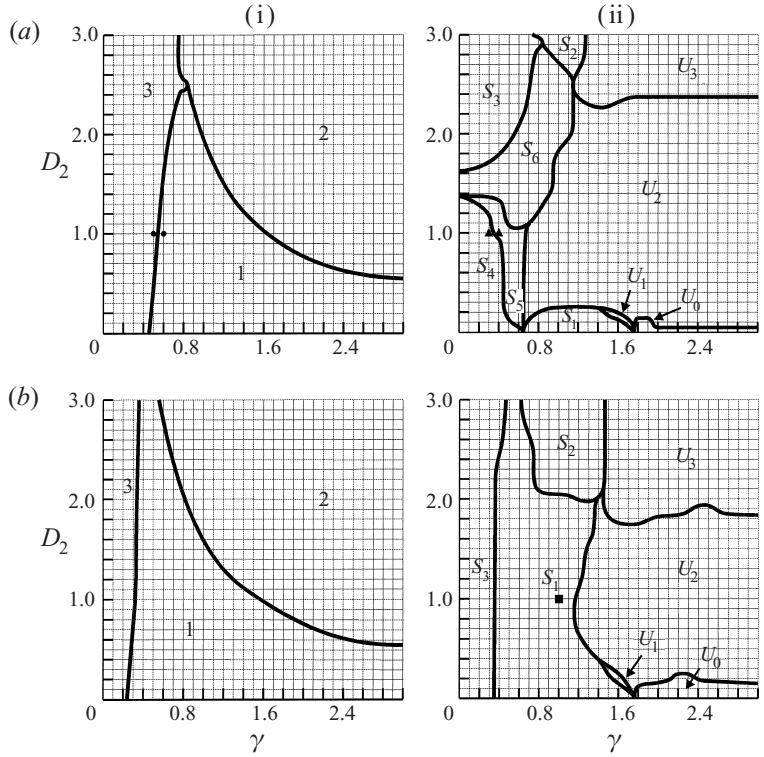


FIGURE 11. Diagrams in the $(\gamma, D_2)$-plane ($0.1 \leqslant \gamma \leqslant 3$; $0 \leqslant D_2 \leqslant 3$) of the states of the system consisting of two hetons at $D_1 = 0$: (*a*) $B = 1.5$; (*b*) $B = 2.5$. (i) Discrete hetons: Region 1, initial movement of the hetons in the same direction and their subsequent scattering; Region 2, movement of the hetons in the same direction; Region 3, 'vortex game'. (ii) Finite-core hetons: Region $S_1$, hetons briefly approach each other, then scatter; Region $S_2$, moving away of both hetons in the same direction; Region $S_3$, 'vortex game'; Region $S_4$, merging of vortex patches (absorption) and their movement in the initial direction of the incident heton; Region $S_5$, the same as $S_4$, but with formation of satellite-vortices; Region $S_6$, the same as Region $S_3$, but with merging of vortex patches and their subsequent division into unequal parts; Region $U_0$, the same as Region $S_1$, but with collapsing of both dipoles; Region $U_1$, the same as Region $S_1$, but with collapsing of the incident dipole into two hetons; Region $U_2$, the same as Region $S_1$, but with intermediate merging of the vortex patches in the layers; Region $U_3$, 'splitting' of the motionless heton by the incident heton. The meaning of the markers is explained in the captions for figures 12, 13 and 14.

sum of the velocities of both dipoles and the value $X = x_1^1 + x_1^2 \equiv -(x_2^1 + x_2^2)$ are invariant. This is an illustration of the first integral (equations (6) and (7)), i.e. of the momentum conservation. An example of movement of this type is plotted in figure 12(*b*). When both hetons run in the same direction, the movement is referred to as type 2. In this case, the asymptotic constant velocity of the initially motionless heton is greater than the velocity of the incident dipole, so it becomes unattainable for this dipole. Figures are not significant and therefore not shown here. Note that the domain of type 3 movements is localized in the zone of small values for the parameter $\gamma$ (large deformation radii) and becomes narrower as the initial distance between the centres of motionless and incident hetons (parameter $B$) increases. For $\gamma \geqslant 2$, either heton scattering or movement in the same direction is possible, the behaviour of the boundary between the domains for these solutions does not really depend on parameter $B$. It is important to note that unstable stationary states correspond to

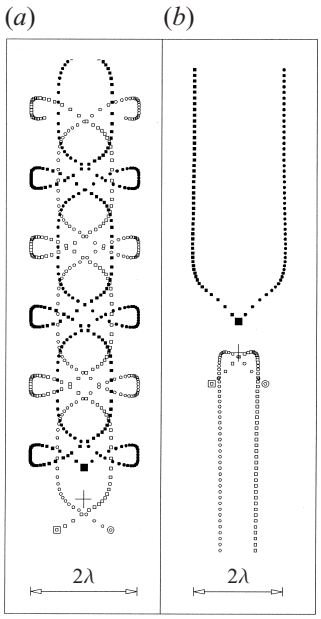


FIGURE 12. Evolution of two discrete hetons at $B = 1.5$, $D_1 = 0$, $D_2 = 1$: (*a*) $\gamma = 0.5$; (*b*) $\gamma = 0.6$. The initial locations of the vortices are shown by the larger markers (black circles in figure 11(*a*)(ii)).

the points on this boundary. In these states, the roles of the hetons change: the motionless vortex starts its movement with the velocity that the initial heton had before it stopped.

3.2.2. *Finite-core hetons*

Interaction between finite-core vortices is much more complicated than that between discrete ones, as shown in figure 11(ii). It may be noted that when the hetons are significantly distant from one another at the initial instant, the qualitative behaviour of point and finite-core hetons is quite similar when $\gamma < 0.8$. However, in the domain where $\gamma \geqslant 0.8$, qualitative differences exist. At $B = 1.5$, differences exist even for small values of $\gamma$. This is related to the merging of close finite-core hetons.

Let us consider some different scenarios of finite-core heton interactions, when one heton is motionless in the initial stage and the other collides with it head-on.

Two types of interaction are shown in figure 13, when $B = 1.5$ and $D_2 = 1$. Figure 13(*a*), where $\gamma = 0.3$, demonstrates the prototype of the 'vortex game' process, when vortex patches in each layer merge (type $S_4$). Then, after cut-off has occurred and thin vortex filaments have been washed out, a dipole of quasi-elliptical vortices is obtained, moving in the same direction as the initial incident heton. In this way, the incident heton absorbs the motionless heton and pulls it in its direction of movement. A new interesting type of movement, $S_5$, when $\gamma = 0.4$, is shown in figure 13(*b*). A heton with a tilted axis moves in a translational manner with small-scale upper-layer anticyclones and lower-layer cyclones rotating in opposite directions along its periphery.

The investigation of the impact of a vortex dipole on the motionless heton is concluded with three examples, calculated for $B = 2.5$. Figure 14 demonstrates a partial case of vortex dipole scattering (type $S_1$). Here, as a result of interaction, the incident heton minimizes the inclination of its axis to practically zero and stops. At the same time, the previously motionless heton adopts an inclined axis and moves away.

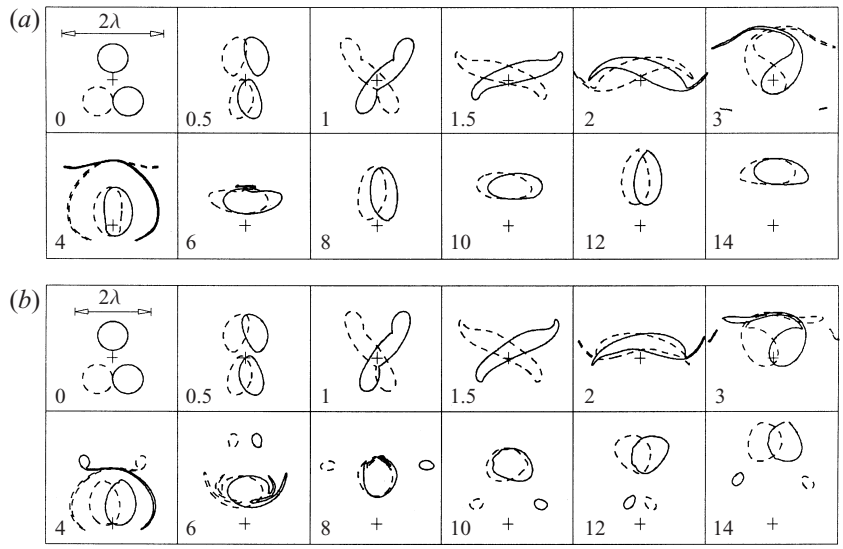


FIGURE 13. Evolution of two finite-core hetons at $B = 1.5$, $D_1 = 0$, $D_2 = 1$: (*a*) $\gamma = 0.3$; (*b*) $\gamma = 0.4$ (black triangles in figure 11(*a*)(ii)).

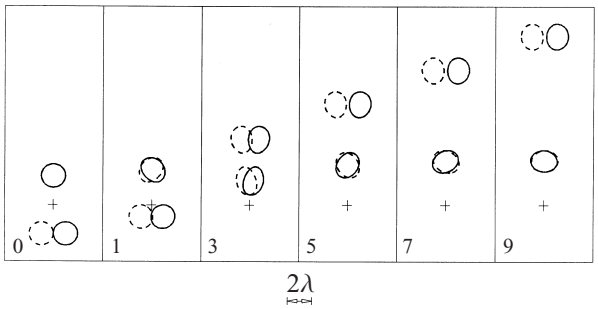


FIGURE 14. Evolution of two finite-core hetons at $B = 2.5$, $D_1 = 0$, $D_2 = 1$, $\gamma = 1$ (black box in figure 11(*b*)(ii)).

This phenomenon is analogous to a 'klapstoss' billiards shot, where, after collision, the moving ball and the motionless ball exchange roles. As mentioned above, such a solution is unstable within the limits of the problem of point-vortex movement. In the case of finite-core vortices, the problem of the stability of this state needs special examination. Nevertheless, calculations show the robustness of such a state. A fairly large domain of parameters ($1.1 \geqslant \gamma \geqslant 0.8$; $1.9 \geqslant D_2 \geqslant 0.9$) in figure 11(*b*)(ii) corresponds to the solutions in the 'klapstoss' class.

### 3.3. *Two vortices with tilted axes: the case of head-on collision* ($D_1 = D_2 \equiv D > 0$)

As in the previous subsection, we will examine two specific cases: $B = 1.5$ and $B = 2.5$.

#### 3.3.1. *Discrete vortices*

A diagram of the possible states of the system (consisting of two point hetons) during head-on collision is given in figure 15(i). This diagram shows that the $(\gamma, D)$-plane is divided into subspaces corresponding to three classes of movement. Two of them are infinite and are characterized by a short initial stage of movement in an

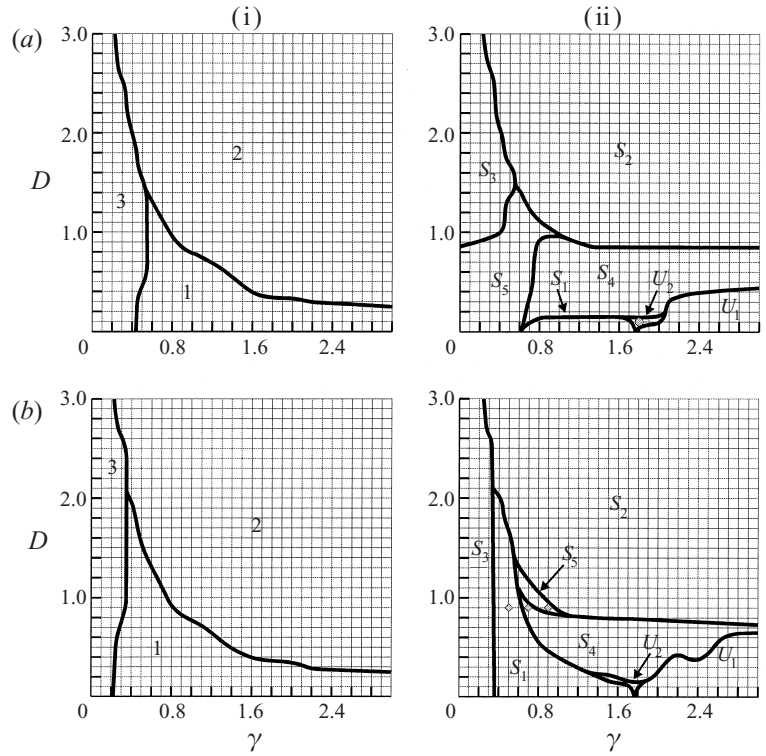


FIGURE 15. Diagrams in the $(\gamma, D)$-plane $(0.1 \leqslant \gamma \leqslant 3,\ 0 \leqslant D \leqslant 3)$ of the states of the system consisting of two hetons at $D_1 = D_2 \equiv C$: (*a*) $B = 1.5$; (*b*) $B = 2.5$. (i) Discrete hetons: Region 1, initial convergence of the hetons and their subsequent scattering; Region 2, initial convergence of the hetons with subsequent exchange with partners and scattering of new dipoles in the normal direction; Region 3, connected state with layerwise vortex rotation along closed O-shaped trajectories in the opposite directions. (ii) Finite-core hetons: Region $S_1$, initial convergence of the hetons and their subsequent scattering; Region $S_2$, initial convergence of the hetons with subsequent exchange with partners and scattering of new dipoles in the normal direction; Region $S_3$, initial convergence of the hetons with subsequent formation of finite state consisting of layerwise vortices rotating along closed O-shaped trajectories in the opposite directions; Region $S_4$, intermediate merging of vortex dipoles and their subsequent division; Region $S_5$, the same as Region $S_3$, but with merging of vortex patches, or with periodic merging and division of vortex patches; Region $U_1$, breaking down of the hetons into non-compensated vortices with their subsequent merging and regrouping into the system of scattering hetons of smaller scales; Region $U_2$, breaking down of each heton into two dipoles with subsequent formation of a structure consisting of two scattering hetons and a central vortex formation grouped together. The meaning of the markers is explained in the captions for figures 16, and 17.

opposite direction. During this stage, in the first case (type 1), both hetons change the signs of axis inclination. Then, the two-layer vortices drift away in opposite directions along a straight line corresponding to the axis of symmetry of the figure. In the second case (type 2), the anticyclones of the upper-layer unite with cyclones of the opposite hetons (the exchange with partners takes place). Then, the newly formed two-layer dipoles move in opposite directions along the straight line perpendicular to the axis of symmetry. The third, which is finite (type 3), includes the movement of upper and lower layer vortices along closed trajectories in directions corresponding to their cyclonicity. These types of motion are covered adequately by Hogg & Stommel (1985*a*).

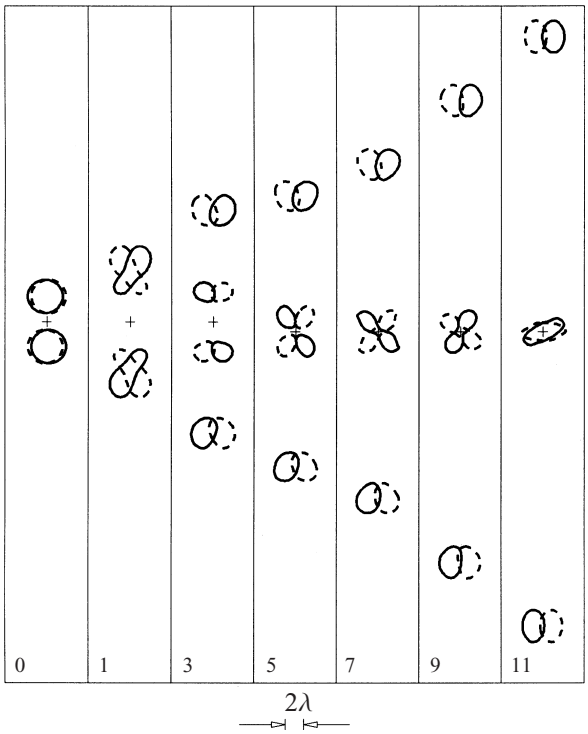


FIGURE 16. Evolution of two finite-core hetons at $B = 1.5$, $D = 0.1$, $\gamma = 1.8$ (grey circles in figure 15(*a*)(ii)).

3.3.2. *Finite-core hetons*

The possible states of hetons with finite cores are shown in figure 15(ii). Here, the pattern of heton interaction is much more complicated. Besides the three types of movement common to the discrete vortices, there are some new types related to the ability of finite-core vortices to merge and collapse. As in § 3.2, the distance $B$ between the heton centres significantly affects the character of their interaction in the lower left-hand quadrant of the given domain of parameters $\gamma$ and $D$. The examples described below demonstrate the different kinds of heton interaction corresponding to this diagram.

Figure 16 shows an example of type $U_2$. It illustrates the intermediate process which is close to those processes shown in figures 9(*c*) and 10(*a*), and results from the interaction of two hetons with initially vertical axes. (All these calculations were performed for $\gamma = 1.8$). In the two cases cited above, the approaching small-scale hetons either moved perpendicularly or, having exchanged partners, moved away in opposite directions, as when an inelastic collision occurs. In this case, the vortex patches in each layer merged and formed a single, motionless connected rotational vortex structure consisting of an upper-layer anticyclone and a lower-layer quasi-elliptical cyclone. This configuration appears to have a quasi-stationary character.

The difference between this situation and that shown in figures 9(*c*) and 10(*a*) can be explained in a similar way. The division of patches in each heton occurs at $y = \pm 2.59$ and, immediately prior to merging, the centres of the vortices in each dipole are separated by an even smaller distance than that in figure 10(*a*) ($x = \pm 0.53$). In this case, merging appears to be more effective.

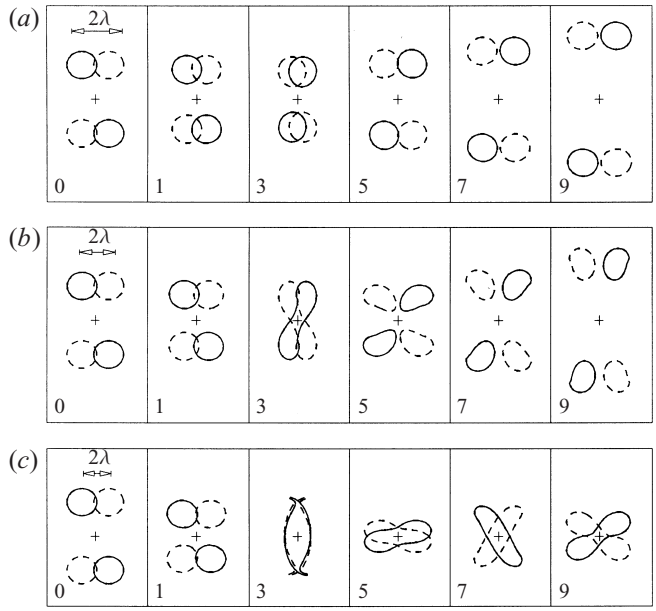


FIGURE 17. Evolution of two finite-core hetons at $B = 2.5$, $D = 0.9$: (*a*) $\gamma = 0.5$; (*b*) $\gamma = 0.7$; (*c*) $\gamma = 0.9$ (grey diamonds in figure 15(*b*)(ii)).

Examples of three different kinds of interaction are shown in figure 17, where the inclination of the heton axis is fixed ($D = 0.9$), $B = 2.5$ and the parameter $\gamma$ varies. Figures 17(*a*), 17(*b*) and 17(*c*) demonstrate the evolution of two hetons for movement types $S_1, S_4$ and $S_5$, respectively.

Thus, figures 16 and 17 represent some typical examples of possible interactions between two finite-core hetons in a symmetrical head-on collision, within the space of external parameters.

It is interesting to note that, at first glance, the formation of the connected state as a result of vortex patch merging following the head-on collision of hetons (figure 17(*c*), type $S_5$) could be considered as the reverse process of the decay of a two-layer unstable vortex (figure 3*a*). In fact, this is not true. The diagrams in figure 15(ii) show that movements of type $S_5$ can only occur when $\gamma < 1$ (i.e. for relatively small vortices, or with strong stratification), but heton decay takes place only when $\gamma > 1.7$ (larger vortices or weak stratification).

## 4. Conclusion

The analysis of the diagrams in figures 8, 11, 15 shows that during any kind of interaction of relatively small vortex patches ($\gamma \leqslant 1.7$), finite-core hetons qualitatively behave like discrete hetons if the distance between the centres of the vortex structures is at least $> 4\lambda$. The dynamics of discrete hetons has been studied quite extensively (Hogg & Stommel 1985*a*, *b*; Gryanik 1983, 1990; Gryanik & Tevs 1989, 1997). The results of calculations conducted within the framework of the discrete model presented in this paper provide a fresh illustration of the corresponding reasoning. Much less is known about the behaviour of finite-core hetons. We have attempted to answer a number of questions and a summary of the main results is presented below.

In accordance with the theory of linear stability, a solitary axially symmetric heton is

| Initial state | Final state | Figure | Parameters |
|---|---|---|---|
| Two motionless two-layer vortices | Formation of scattering smaller heton with titled axis | 9(*c*) | $B = 1.5, D = 0, \gamma = 1.8$ |
| | | 10(*a*) | $B = 1.7, D = 0, \gamma = 1.8$ |
| Vortex with tilted axis incident on the motionless heton | 'Absorption' and drift of motionless heton | 13(*a*) | $B = 1.5, D_1 = 0, D_2 = 1, \gamma = 0.5$ |
| | Formation of the two-layer vortex dipoles, accompanied in their movements by rotating satellites | 13(*b*) | $B = 1.5, D_1 = 0, D_2 = 1, \gamma = 0.4$ |
| | Formation analogous to 'klapstoss' billiard shot | 14 | $B = 1.5, D_1 = 0, D_2 = 1, \gamma = 1$ |
| Head-on symmetrical collision of two-layer dipoles with tilted axes | Formation of the configuration consisting of a motionless two-layer vortex formation and di-poles drifting away from it | 16 | $B = 1.5, D = 0.1, \gamma = 1.8$ |
| | Formation of motionless connected two-layer vortex | 17(*c*) | $B = 2.5, D = 0.9, \gamma = 0.9$ |

TABLE 1.

neutrally stable when $\gamma \leqslant 1.7$ (remember that equal layer thicknesses are considered). If $\gamma > 1.7$, the heton becomes unstable and, as it develops, breaks into a two-layer dipole which subsequently scatters. The resulting structures coincide with the most unstable modes. A necessary condition for the formation of a tripolar structure – as a result of instability – is the presence of a non-zero barotropic component.

The heton with a tilted axis moves uniformly forward (this is the translational stationary state, studied in detail by Polvani 1991) whatever the inclination of its axis, if $\gamma \leqslant 1.7$. If $\gamma > 1.7$, the stationary state is possible only when $D > 0.5$. When $D \leqslant 0.5$, the moving two-layer vortex breaks, forming smaller hetons that move in different directions along the axis of symmetry. Areas with stable and unstable states of the heton with tilted axis are shown in figure 6. The properties of a single heton given above strongly determine the character of interaction between two or more hetons. Judging from the results of numerous calculations performed for the symmetrical interaction between two hetons, a wide variety of possible movements may exist for a vortex system, depending on the dimensions of vortex patches (parameter $R$), their initial position (parameters $B, D_1, D_2$), and stratification (parameter $\gamma$). The diagrams in figures 8, 11, 15 summarize these results. The illustrations show that in all the types of interaction examined, the most complicated, in the dynamic sense, are the regimes of the intermediate stages. As a rule, these result in newly formed quasi-stationary states. The most interesting of them are shown in table 1.

The intermediate stages noted above, which include the stages of vortex patch division and merging, may have implications for oceanic processes. Generally, their timescales are a few units of dimensionless time, so that their input into the synoptic variability of the region can be very important. In light of what has been stated above, the 'klapstoss' type of configuration (figure 14) may be regarded as an example of a quasi-stationary regime. It should also be noted that the processes of vortex merging and division play a key role in the understanding of the drifting and mixing mechanisms of different water masses. It should be emphasized that intermediary

processes of vortex patch division and merging have an 'inelastic' character, and the transition to new quasi-equilibrium states occurs in accordance with the principle of 'adiabatic steadiness' (Dritschel 1995). As a rule, as seen in most of the figures, the intermediary stages of vortex interaction are accompanied by intense filamentation. Consequently, incomplete merging of vortices is more often encountered. On the other hand, figures 9(*b*), 14 and 17(*a*) are examples of 'elastic' interaction.

Let us consider variations in parameter $\gamma$ for some ocean vortex structures. Kamenkovich *et al.* (1986) have shown that for Gulf Stream rings in the northern part of the Sargasso Sea, at depths of 500–1200 m, $\lambda = 40$ km and the vortex radii are between 75 and 125 km. These values correspond to $\gamma$ ranging between 1.9 and 3.1. On the basis of observational data given in the same book, the parameter $\gamma$ can also be estimated for other regions: $\gamma = 3.1$ for the vortex in the region of Eastern-Australian Current; $\gamma = 1.7$ in the south part of the Norwegian Sea; $\gamma = 1.5$ for an anticyclonic vortex in the region of station North Pole-23 in the Arctic basin; $\gamma = 1.2$ for the central part of Drake Passage. Griffiths & Hopfinger (1987) note that for Gulf Stream warm-core rings, $1.7 < \gamma < 3.3$. According to Carton & Corréard (1997), for Bay of Biscay rings, $1.3 < \gamma < 2.3$. Finally, Hopfinger & van Heijst (1993) estimate the characteristic values for the ocean at $0.7 < \gamma < 2$. Processes shown in figures 3, 4, 5, 9(*c*), 14, 16 and 17(*c*) correspond to these intervals of parameter $\gamma$.

The configurations corresponding to figures 9(*a*), 9(*b*), 12, 13(*a*), 13(*b*), 17(*a*) and 17(*b*) may contribute to a better understanding of vortex processes in lakes. According to Filatov (1983), in the case of deep lakes such as Baikal and Ladozhskoye, vortex radii change in the range of 920 to 3360 m and $\lambda = 5$–10 km. Therefore, it appears that $\gamma = 0.09$–0.67.

Thus, it can be seen that the greater part of the interval examined in this study, namely $0.1 \leqslant \gamma \leqslant 3$, corresponds to real stratification values in lake and oceanographic problems. Most of the results obtained may therefore have some implications for the interpretation of real vortex movement in natural water reservoirs.

This study was made possible through financial support from INTAS (Grant 94-3614). Support for the M. A. S. was also provided by RFBR (Grant 98-05-65446). Discussions with Drs V. F. Kozlov, P. A. Davies, E. J. Hopfinger, V. M. Gryanik, V. N. Zyryanov, Z. I. Kizner and X. Carton were very helpful and most appreciated. Finally, we would like to thank Mrs O. I. Yakovenko for her technical assistance.

## Appendix A

In order to obtain more information about the stability analysis conducted for a two-layer vortex in KMS, let us examine the special case when the vortex is a heton, i.e.

$$h_1 \Pi_1^1 + h_2 \Pi_2^1 = 0, \tag{A 1}$$

where for dimensionless layer depths the relation $h_1 + h_2 = 1$ is valid. The formula (A 1) makes it possible to introduce the parameter $\mu$ using the relations

$$\Pi_1^1 = h_2 \mu = (1 - h_1)\mu,$$

$$\Pi_2^1 = -h_1 \mu.$$

As mentioned in § 2.1, the problem of vortex stability reduces to the solution of the system of linear algebraic equations for $\epsilon_i$ from (4). Since the determinant of this

system is equal to zero, this gives the dispersion equation:

$$\delta_m = \tfrac{1}{2}\mu[(1-2h_1)(L_1(\gamma)-L_m(\gamma)) \pm \sqrt{\Phi_m(\gamma,h_1)}],$$

where

$$L_m(\gamma) = I_m(\gamma)K_m(\gamma),$$

$$\Phi_m(\gamma,h_1) = [L_1(\gamma)-L_m(\gamma)] \times \left[L_1(\gamma)-(1-2h_1)^2 L_m(\gamma) - \frac{2}{m}h_1(1-h_1)\right]. \qquad \text{(A 2)}$$

The relation, $\Phi_m < 0$, is the necessary condition of instability. $L_m(\gamma)$ is known (Abramowitz & Stegun 1972) to be a monotonously decreasing function of both the argument $\gamma$ and the number $m$. Moreover,

$$L_m(\gamma) \to \tfrac{1}{2}m \quad \text{at} \quad \gamma \to 0,$$

$$L_m(\gamma) \to \tfrac{1}{2}\gamma \quad \text{at} \quad \gamma \to \infty.$$

From (A 2), it follows that $\Phi_1(\gamma,h_1) \equiv 0$, i.e. the first mode is always neutrally stable. By making the second term in square brackets in (A 2) equal to zero, we obtain:

$$h_1 = \frac{1}{2}\left\{1 \pm \left[\frac{1/2m - L_1(\gamma)}{1/2m - L_m(\gamma)}\right]^{1/2}\right\}.$$

When $h_1 = \frac{1}{2}$, as discussed in this article, the following relation should be fulfilled

$$L_1(\gamma) = \frac{1}{2m}. \qquad \text{(A 3)}$$

Let the solution of equation (A 3) be represented as $\gamma_m$, corresponding to the mode with number $m$. Then $\gamma_m \sim m$ at $m \gg 1$. From the numerical solution of (A 3) we have approximately:

$$\gamma_2 = 1.705, \quad \gamma_3 = 2.840, \quad \gamma_4 = 3.893, \quad \gamma_5 = 4.919, \quad \gamma_6 = 5.934.$$

Thus, if $n > 2$ at $\gamma_n < \gamma < \gamma_{n+1}$, the unstable modes are those with numbers $m = 2, 3, \ldots, n$ (see, for example, figure 2).

## Appendix B

The main idea of the CDM for the case of two layers is expressed in the statement: if we have a set of simply-connected domains $S_i^j$ with contours $C_i^j$, and PV takes constant values $\Pi_i^j$ different from zero only inside them, the velocity of any fluid particle will be completely determined by the shape of the contours $C_i^j$. In our case, the movement of nodes along the contours $C_i^j$ is governed by the equations

$$\frac{\mathrm{d}(\boldsymbol{r}_i^j)_n}{\mathrm{d}t} = (\boldsymbol{V}_i^j)_n \quad (n = 1, \ldots, N_i^j, \quad j = 1, \ldots, J_i, \quad i = 1, 2) \qquad \text{(B 1)}$$

which should be supplied with initial conditions

$$t = 0, \quad (\boldsymbol{r}_i^j)_n = (\boldsymbol{r}_i^j)_n^0. \qquad \text{(B 2)}$$

Here, $(\boldsymbol{r}_i^j)_n$ is the radius-vector of the fixed particle $n$ over the contour $j$ of the layer $i$; $N_i^j$ is the number of particles on the contour $j$ in the layer $i$; $J_i$ is the number of contours in the layer $i$.

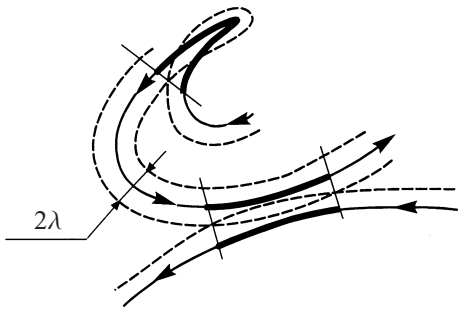


FIGURE 18. Sketch of the contour surgery algorithm (according to Makarov 1991).

Expressions for velocities which enter into the right-hand sides of (B 1) contain contour integrals, and the only unknown quantities are the configurations of the evolving contours.

During the numerical modelling of vortex patch movement, equations (B 1) are solved with respect to the nodes selected according to initial conditions (B 2). The system of ordinary differential equations (B 1) was solved with the fourth-order Runge–Kutta method using the Gill 'optimum' formula for timestepping (Hairer, Nørsett & Wanner 1987). The algorithm is used to study the evolution of two-layer vortex structures in the special case of $h_1 = h_2 = 0.5$ (equal layer thicknesses). A typical initial number of nodes is 60 for a circle of unit radius. During the calculation, this number increases proportionally with the length of the contour; new nodes uniformly redistribute themselves along the contour. In some simulations, 100 or 120 initial nodes were taken to ensure accuracy. When modelling the decay process for unstable two-layer vortices (§ 2.1), the initial conditions (B 2) are also formulated for each layer for the set of nodes distributed uniformly along the circular contours of vortex patches of unit radii. The source of perturbations could be no more than 'computer noise', intrinsic to any numerical calculations. The approximation, interpolation, numerical differentiation and grid integration procedures were carried out using the periodic cubic spline techniques (Kozlov 1983).

We also applied the contour surgery scheme (Makarov 1991) which is based on geometrical criteria like that proposed by Dritschel (1988). Contour surgery makes it possible to cut out vorticity filaments and remove the unnecessary parts of the boundaries which appear when vortices with the same potential vorticity values approach each other. The main idea of the algorithm is to construct auxilliary contours at a distance of $\epsilon$ on each side of every real contour, and to determine the points of their intersection. The cut-off of the excess parts of the real contour occurs as shown in figure 18. The removable parts of the contours are marked by the bold line. Makarov (1991) determined that a reasonable accuracy of calculations is obtained at $\epsilon \leqslant 0.1h$, where $h$ is a step between neighbouring nodes of the contour. In particular, Makarov showed for the example case of the unstable shielded vortex evolution that when $h = 0.078$, $\Delta t = 0.1$, $\epsilon = 0.006$, the errors on the integral invariants such as the circulation $\Gamma$ and the momentum $J$ are of 2%, and 2%, respectively, at $t = 18$ and 6% and 7.6% at $t = 20$. If, for example, the initial number of the nodes is 60 ($h \simeq 0.105$) we chose $\epsilon = 0.01$.

## Appendix C

The formula for translational movement of the discrete heton (5) takes the form:

$$v(z) = \frac{\gamma s_1^1}{4\pi}\phi(z) \quad \text{where} \quad \phi(z) = \frac{1}{z} - K_1(z).$$

It is easy to see that for the derivative

$$f(z) \equiv \phi'(z) = K_0(z) + \frac{1}{z}K_1(z) - \frac{1}{z^2},$$

which is a monotonous decreasing function, the following estimates are valid:

$$f(z) \sim -\ln z > 0 \quad \text{at } z \ll 1,$$

$$f(z) \sim -\frac{1}{z^2} < 0 \quad \text{at } z \gg 1.$$

Thus, $f(z)$ changes its sign at some point $z^*$ in the interval $(0, \infty)$. The transcendental equation $f(z) = 0$ has the approximate solution $z = z^* = 1.114$. As to the function $\phi(z)$ itself, it is non-negative, has a unique maximum at $z = z^*$ and, moreover,

$$\phi(z) \sim -z \ln z \to 0 \quad \text{at } z \ll 1,$$

$$\phi(z) \sim \frac{1}{z} \to 0 \quad \text{at } z \gg 1.$$

## REFERENCES


Abramowitz, M. & Stegun, I. A. (Ed.) 1972 *Handbook of Mathematical Functions*. Dover.

Carton, X. J. & Corréard, S. M. 1997 Baroclinic tripolar geostrophic vortices: formation and subsequent evolution. In *Proc. IUTAM/SIMFLOW Symp.* Lyngby, Denmark. Kluwer.

Cheney, R. E., Gemmill, W. H., Shank, M. K., Richardson, P. L. & Webb, D. 1976 Tracking a Gulf Stream ring with SOFAR floats. *J. Phys. Oceanogr.* **6**, 741–749.

Corréard, S. M. & Carton, X. J. 1997 Vertical alignment of geostrophic vortices: on the influence of the initial distribution of potential vorticity. In *Proc. IUTAM/SIMFLOW Symp.*, Lyngby, Denmark. Kluwer.

Cresswell, G. R. 1982 The coalescence of two East Australia Current warm-core eddies. *Science* **215**, 161–164.

Cushman-Roisin, B., Sutyrin, G. G. & Tang, B. 1992 Two-layer geostrophic dynamics. Part I: Governing equations. *J. Phys. Oceanogr.* **22**, 117–127.

Dritschel, D. G. 1988 Contour surgery: a topological reconnection scheme for extended integrations using contour dynamics. *J. Comput. Phys.* **77**, 240–266.

Dritschel, D. G. 1995 A general theory for two-dimensional vortex interactions. *J. Fluid Mech.* **293**, 269–303.

Filatov, N. N. 1983 *Dynamics of Lakes*. Leningrad, Gidrometeoizdat. 168 pp. (In Russian.)

Griffiths, R. W. & Hopfinger, E. J. 1986 Experiments with baroclinic vortex pairs in a rotating fluid. *J. Fluid Mech.* **173**, 501–518.

Griffiths, R. W. & Hopfinger, E. J. 1987 Coalescing of geostrophic vortices. *J. Fluid Mech.* **178**, 73–97.

Gryanik, V. M. 1983 Dynamics of singular geostrophic vortices in a two-level model of atmosphere (ocean). *Izv. Atmos. Ocean. Phys.* **19**, 227–240 (in Russian), 171–179 (English translation).

Gryanik, V. M. 1990 About theoretical models of the localized quasi-geostrophic eddies in the atmosphere and ocean. In *The Investigations of Vortex Dynamics and Energetics of the Atmosphere, and the Problems of Climate* (ed. E. G. Nikiforov & V. F. Romanov) pp. 31–60. Leningrad, Gidrometeoizdat. (In Russian.)

Gryanik, V. M. & Tevs, M. V. 1989 Dynamics of singular geostrophic vortices in an $N$-layer model of atmosphere (ocean). *Izv. Atmos. Ocean. Phys.* **25**, 243–256 (in Russian), 179–188 (English translation).

Gryanik, V. M. & Tevs, M. V. 1997 Dynamics and energetics of heton interacting in linearly and exponentially stratified media. *Izv. Atmos. Ocean. Phys.* **33**, 419–433 (in Russian), 385–398 (English translation).

Hairer, E., Nørsett, S. R. & Wanner, G. 1987 *Solving Ordinary Differential Equations. – I: Nonstiff Problems.* Springer.

Helfrich, K. R. & Send, U. 1988 Finite-amplitude evolution of two-layer geostrophic vortices. *J. Fluid Mech.* **197**, 331–348.

Hogg, N. G. & Stommel, H. M. 1985*a* The heton, an elementary interaction between discrete baroclinic geostrophic vortices, and its implications concerning eddy heat-flow. *Proc. R. Soc. Lond.* A **397**, 1–20.

Hogg, N. G. & Stommel, H. M. 1985*b* Hetonic explosions: the breakup and spread of warm pools as explained by baroclinic point vortices. *J. Atmos. Sci.* **48**, 1465–1476.

Hopfinger, E. J. & van Heijst, G. J. F. 1993 Vortices in rotating fluids. *Ann. Rev. Fluid Mech.* **25**, 241–289.

Ikeda, M. 1981 Instability and splitting of mesoscale rings using a two-layer quasi-geostrophic model on an f-plane. *J. Phys. Oceanogr.* **11**, 987–998.

Kamenkovich, V. M., Koshlyakov, M. N. & Monin, A. S. 1986 *Synoptic Eddies in the Ocean.* Reidel, 460 pp.

Kennelly, M. A., Evans, R. H. & Joyce, T. M. 1985 Small-scale cyclones on the periphery of Gulf Stream warm-core ring. *J. Geophys. Res.* **90**, 8845–8857.

Kozlov, V. F. 1983 The method of contour dynamics in model problems of the ocean topographic cyclogenesis. *Izv. Atmos. Oceanic Phys.* **19**, 845–854 (in Russian), 635–640 (English translation).

Kozlov, V. F. & Makarov, V. G. 1985 Simulation of the instability of axisymmetric vortices using the contour dynamics method. *Fluid Dyn.* **1**, 33–39 (in Russian), 28–34 (English translation).

Kozlov, V. F., Makarov, V. G. & Sokolovskiy, M. A. 1986 Numerical model of the baroclinic instability of axially symmetric eddies in two-layer ocean. *Izv. Atmos. Ocean. Phys.* **22**, 868–874 (in Russian), 674–678 (English translation) (referred to herein as KMS).

Legras, B. & Dritschel, D. G. 1993 A comparison of the contour surgery and pseudo-spectral method. *J. Comput. Phys.* **104**, 287–302.

McWilliams, J. C. 1984 The emergence of isolated coherent structures in turbulent flow. *J. Fluid Mech.* **146**, 21–43.

Makarov, V. G. 1991 Computational algorithm of the contour dynamics method with changeable topology of domains under study. *Model. Mech.* **5(22)**, 83–95. (In Russian.)

Makarov, V. G. 1996 Numerical simulation of the formation of tripolar vortices by the method of contour dynamics. *Izv. Atmos. Ocean. Phys.* **32**, 46–55. (In Russian.)

Morel, Y. G. & Carton, X. J. 1994 Multipolar vortices in two-dimensional incompressible flows. *J. Fluid Mech.* **267**, 23–51.

Nof, D. & Simon, L. M. 1987 Laboratory experiments on the merging of nonlinear anticyclonic eddies. *J. Phys. Oceanogr.* **17**, 343–357.

Pedlosky, J. 1987 *Geophysical Fluid Dynamics*, 2nd edn. Springer. 710 pp.

Polvani, L. M. 1991 Two-layer geostrophic vortex dynamics. Part 2. Alignment and two-layer V-states. *J. Fluid Mech.* **225**, 241–270.

Polvani, L. M., Zabusky, N. J. & Flierl, G. R. 1988 Applications of contour dynamics to two-layer quasi-geostrophic vortices. *Fluid Dyn. Res.* **3**, 422–424.

Polvani, L. M., Zabusky, N. J. & Flierl, G. R. 1989 Two-layer geostrophic vortex dynamics. Part 1. Upper-layer V-states and merger. *J. Fluid Mech.* **205**, 215–242.

Richardson, P. L., Maillard, C. & Stanford, T. B. 1979 The physical structure and life history of cyclonic Gulf Stream ring Allen. *J. Geophys. Res.* **84**, 7727–7741.

Robinson, A. R., Carton, J. A., Pinardi, N. & Mooers, C. N. K. 1986 Dynamical forecast and dynamical interpolation: an experiment in the California Current. *J. Phys. Oceanogr.* **16**, 1569–1579.

Sokolovskiy, M. A. 1988 Numerical modelling of nonlinear instability for axisymmetric two-layer vortices. *Izv. Atmos. Ocean. Phys.* **24**, 735–743 (in Russian), 536–542 (English translation).

Sokolovskiy, M. A. 1989 Head-on collisions of distributed hetons. *Trans. Dokl. USSR Acad. Sci.* **306**, 198–202 (in Russian), 215–217 (English translation).

Sokolovskiy, M. A. 1990*a* Numerical modelling of the interaction of distributed hetons during

their head-on collisions. In *Method of contour dynamics in oceanological investigations* (ed. V. F. Kozlov), pp. 40–57. Vladivostok. FED USSR Acad. Sci. (In Russian.)

Sokolovskiy, M. A. 1990*b* *On the interaction of distributed hetons*. Preprint. Vladivostok. POI FED USSR Acad. Sci. 20pp. (In Russian.)

Sokolovskiy, M. A. 1997*a* Stability of an axisymmetric three-layer vortex. *Izv. Atmos. Ocean. Phys.* **33**, 19–30 (in Russian), 16–26 (English translation).

Sokolovskiy, M. A. 1997*b* Stability analysis of the axisymmetric three-layered vortex using contour dynamics method. *Comput. Fluid Dyn. J.* **6**, 133–156.

Valcke, S. & Verron, J. 1993 On interactions between two finite-core hetons. *Phys. Fluids* A **5**, 2058–2060.

Valcke, S. & Verron, J. 1996 Cyclone-anticyclone asymmetry in the merging process. *Dyn. Atmos. Oceans* **24**, 227–236.

Valcke, S. & Verron, J. 1997 Interaction of baroclinic isolated vortices: the dominant effect of shielding. *J. Phys. Oceanogr.* **27**, 524–541.

Verron, J., Hopfinger, E. J. & McWilliams J. C. 1990 Sensitivity to initial conditions in the merging of two-layer baroclinic vortices. *Phys. Fluids* A **2**, 886–889.

Verron, J. & Hopfinger, E. J. 1991 The enigmatic merging conditions of two-layer baroclinic vortices. *C. R. Acad. Sci. Paris.* **313**, Ser. II, 737–742.

Verron, J. & Valcke, S. 1994 Scale-dependent merging of baroclinic vortices. *J. Fluid Mech.* **264**, 81–106.

Yano, J.-I. & Flierl G. R. 1992 Isolated potential vorticity patches in quasi-geostrophic zonal shear flows. *Dyn. Atmos. Oceans* **16**, 439–472.

Young, W. R. 1985 Some interactions between small numbers of baroclinic, geostrophic vortices. *Geophys. Astrophys. Fluid Dyn.* **33**, 35–61.